Attribution of observed extreme marine wind speeds and associated hazards to midlatitude cyclone conveyor belt jets near the British Isles

Received: 3 August 2022 | Revised: 28 December 2022 | Accepted: 2 January 2023

DOI: 10.1002/joc.7999

International Journal of Climatology RMetS

RESEARCH ARTICLE

Attribution of observed extreme marine wind speeds and associated hazards to midlatitude cyclone conveyor belt jets near the British Isles

Emanuele S. Gentile | **Suzanne L. Gray**

Department of Meteorology, University of Reading, Reading, UK

Correspondence
Emanuele S. Gentile, Department of Meteorology, University of Reading, Reading RG6 6ET, UK.
Email: e.gentile@pgr.reading.ac.uk

Funding information
Natural Environment Research Council, Grant/Award Number: NE/R007640/1

Abstract

Extreme wind speeds, gusts, and wind wave heights associated with midlatitude cyclones pose a hazard to shipping lanes and offshore infrastructure operating in the North Atlantic Ocean seas surrounding the British Isles. Several studies have assessed the variability of wind and waves in this region using reanalyses, but few have used surface observations of extreme wind speeds and wave heights. Here, we use a network of marine surface stations to derive the 2012–2020 climatology of daily maximum wind speed events. An algorithm is used to attribute the extreme wind events, characterized as exceeding the 20 and 25 $m \cdot s^{-1}$ thresholds, to the cyclone warm conveyor belt (WCB), and early (CCBa) and returning (CCBb) cold conveyor belt jets; cyclones are matched with up to 90% of extreme wind events. The CCBb is most frequently associated with the strong wind speeds, accounting for 46 and 59% of the events exceeding the two thresholds, respectively. The CCBb also leads to the largest number of compound wind and wave hazard events (37 out of 87). Although the WCB is associated with the second largest number of extreme wind events, the CCBa accounts for the second largest number of compound extreme wind and wave events (24). The ERA5 reanalysis underestimates the observed extreme wind speeds, and associated gusts and wind-wave heights, during extreme wind events for all the conveyor belt jets. The wind speeds and associated gusts are most underestimated, by median values of 4.5 and 5.5 $m \cdot s^{-1}$, respectively, and similar percentage error ($\approx 25\%$), when associated with the CCBb; however, the wind-wave heights are most underestimated, by a median of 3.4 m, when associated with the CCBa. Hence, while the marine CCBb jet, found in mature cyclones, is both most hazardous and underestimated in the ERA5 near the British Isles, the CCBa jet can be nearly as hazardous when considering compound wind-wave events.

KEYWORDS

compound wind-wave hazard, conveyor belt jets, ERA5 bias, extreme gust, extreme wind speed, midlatitude cyclones, reanalysis, surface observations

1 | INTRODUCTION

Midlatitude cyclones pose a major threat to shipping lanes and offshore installations located in the seas surrounding the British Isles (Bell *et al.*, 2017). Associated strong winds and waves batter wind farms and oil production platforms, leading to structural damage (Cardone *et al.*, 2014). Offshore energy industries and weather centres could benefit from an improved understanding of cyclone features associated with observed extreme surface wind speeds and wind-wave heights: offshore industries could better assess the compound wind-wave risk posed by midlatitude cyclones, while weather centres could better diagnose and attribute biases in model analyses and reanalyses to specific cyclone features. In this paper we present a climatology of observed offshore extreme wind speeds and objectively partition events according to the associated cyclone features.

Many studies have linked the extreme wind speeds observed by land weather stations and by soundings in the mid-troposphere to three different airflows within midlatitude cyclones (Parton *et al.*, 2010; Martínez-Alvarado *et al.*, 2012; Neu *et al.*, 2013; Hewson and Neu, 2015): the warm and cold conveyor belt wind jets (WCB and CCB, respectively) and the sting jet (SJ). These air flows can be represented by the conveyor belt conceptual model (Browning and Roberts, 1994), illustrated in Figure 1a. The WCB originates as a near-surface jet, which can have intense winds, and then ascends over the warm front above the cold air below (Martínez-Alvarado *et al.*, 2014). However, some of the strongest and most damaging surface winds form on the rear, equatorward flank of midlatitude cyclones, when the CCB jet wraps around the low-pressure centre and the winds are mixed through the boundary layer producing extreme gusts at the surface, as described in Hewson and Neu (2015). In earth-relative winds, the CCB often appears split into two components due to the jet, which has a easterly system-relative component, opposing the typically northeastwards direction of travel of the cyclone (as shown in Figure 1a). The part of the CCB leading to strong winds on the rear equatorward flank of the cyclone, termed CCBb, is distinct from the early part of the CCB, termed CCBa. The relationship between the wind speed and gust speed associated with strong wind jets is dependent on the stability, and related height, of the boundary layer. The WCB jet occurs in the warm sector of the cyclone which generally has a shallow stable boundary layer. In contrast, the CCB jet (and particularly the CCBb part of it) occurs in the cold sector which typically has a more unstable and deeper boundary layer (see table 2 in Hewson and Neu (2015) for the stability characteristics of the jets and fig. 14 of Sinclair *et al.* (2010) for the height of the boundary layer in the warm and cold sectors of cyclones). Sometimes a finer mesoscale airstream, the SJ, is present in midlatitude cyclones. The SJ exits from the tip of the hook-shaped cloud head and descends to the surface over several hours, producing an additional region of strong winds and exceptionally strong gusts (Clark and Gray, 2018). Besides sting jets, there are also other fine-scale features associated with midlatitude cyclones responsible for damaging surface winds, such as the lines of organized convection that occur along cold frontal boundaries, and (less so) near occluded fronts (Clark, 2013; Earl *et al.*, 2017). The strong wind regions associated with the cyclone conveyor belts are illustrated in Figure 1b for a real-world example cyclone, windstorm Friedhelm (2011), using 10-m wind speeds derived from European Centre for Medium-range Weather Forecasts (ECMWF) fifth generation hourly reanalysis (ERA5). As discussed in Vaughan *et al.* (2015), cyclone Friedhelm deepened spectacularly by 44 hPa between 1200 UTC on December 7 and 1200 UTC on December 8 (while crossing the North Atlantic). Structurally, cyclone Friedhelm resembled a Shapiro–Keyser cyclone (for the diagram of a Shapiro–Keyser cyclone, see Figure 1a). The strongest winds, exceeding 20 $m \cdot s^{-1}$, are associated with the CCB, while the slightly weaker winds, of up to 18–20 $m \cdot s^{-1}$ and located in the warm sector of the cyclone, are associated with the WCB. The CCB flow is initially southeasterly (CCBa), but as the CCB wraps around the cyclone centre (located off the east coast of northern Scotland) it changes from northerly to southwesterly (CCBb). Since the WCB is also characterized by a southwesterly flow, knowledge of the boundary between the cold and the warm sector air masses is required to distinguish between the two features. Previous studies have shown that the CCB and WCB can be easily detected from reanalysis data alone by combining information on location of fronts (e.g., diagnosed from the location of the sharpest equivalent potential temperature gradient) with wind direction (Catto *et al.*, 2015; Hart *et al.*, 2017; Catto and Raveh-Rubin, 2019; Eisenstein *et al.*, 2022; Volonté *et al.*, 2022). The CCB and WCB can also be identified objectively using criteria applied to air parcel trajectories. For example, Madonna *et al.* (2014) used this method to produce a climatology of WCBs using reanalysis data.

Reanalyses are among the most popular datasets for the assessment of both land and marine wind variability. Besides to being easy to use, reanalyses also provide a physically coherent wind field. However, reanalyses' coarse resolution (the highest being $\approx$30 km in the midlatitudes) and boundary-layer parametrization issues (Smart and Browning, 2014) make reanalyses less suitable for detecting wind speed extremes and associated weather hazards, such as high waves (Hewson and

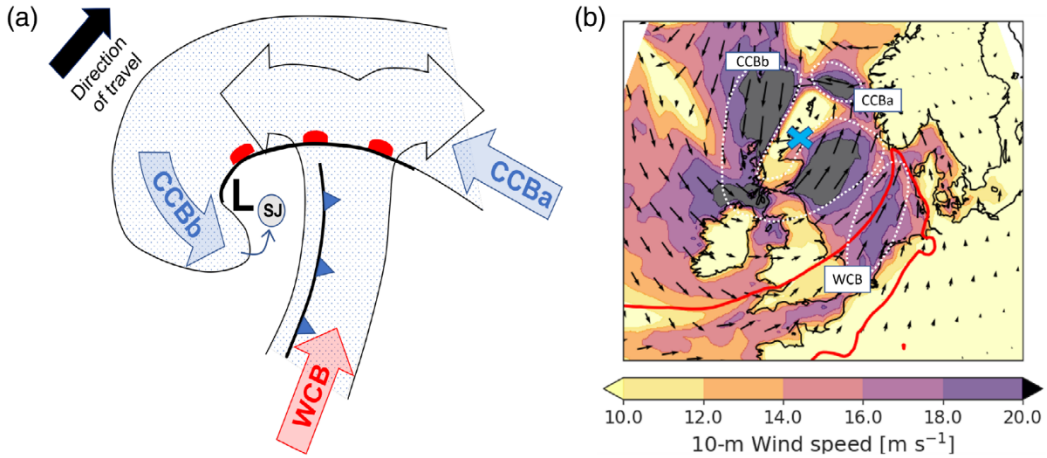

FIGURE 1 (a) Conceptual model of a Shapiro-Keyser cyclone with the WCB, CCBa, and CCBb indicated. Fronts are marked conventionally, "L" indicates the cyclone centre and stippling indicates cloud. (b) Illustration of the conveyor belt jets of cyclone Friedhelm (December 8, 2011, 1700 UTC) using ERA5 data. The jet regions (subjectively identified) are enclosed by white dashed lines and 10-m winds are shown by arrows with speeds shaded. The blue cross indicates the mean sea level pressure minimum of the cyclone, while the thick red line indicates the boundary between the warm and cold sectors (computed by the algorithm developed in this paper detailed in section 2.4)

Neu, 2015; Molina *et al.*, 2021). This shortcoming can be overcome by the use of surface observation data, which, despite their inhomogeneity, have proved useful to investigate extreme wind and wave events (Earl and Dorling, 2013; Bell *et al.*, 2017). Besides surface observations, satellite-derived datasets have also been used to detect weather extremes, such as North Atlantic extreme wave heights (Rulent *et al.*, 2020; Ponce de León and Bettencourt, 2021) though, compared to surface observations, they present the disadvantages of rain contamination, a lack of data near land (usually within $\approx$15 km from the coast), and intermittent temporal sampling (Bourassa *et al.*, 2019).

There are many studies that have investigated the variability of the extreme wind speeds and gusts associated with mesoscale cyclone features by utilizing surface observations over the UK land (Hewston and Dorling, 2011; Earl and Dorling, 2013; Earl *et al.*, 2017). In summary, these studies find that the prevailing direction of strongest winds and daily maximum gusts (DMGS) is westerly (ranging from northwesterly to southwesterly), that $\approx$80% of the extreme observed wind speeds occur in cyclone-dense seasons, and that boundary-layer convective-scale processes and land surface characteristics can control the intensity of observed DMGS. Combining the DMGS observed by a land surface station network for the period 2008–2014 with radar imagery and UK surface pressure charts, Earl *et al.* (2017) manually attributed the recorded DMGS to subsynoptic cyclone features, deriving a statistics of the frequency with which each cyclone feature (WCB, CCB, SJ, convective lines) associated with extreme DMGS.

In contrast to these observation-based wind and gust climatologies focusing on the UK land, only a few studies have focused on the North Sea and other North Atlantic Ocean seas that surround the British Isles. Because of the dearth of historical time series of wind, gust, and wave height observations, these studies have had to rely on model hindcasts, reanalysis data, and just a few surface observations. A common trait of these studies is the focus on wind energy applications rather than on the physical understanding of circulation patterns and wind on gust and wave heights extremes. For example, Geyer *et al.* (2015) investigated the 1958–2012 North Sea surface wind climatology from a model hindcast in order to derive an assessment of the wind power potential, finding a decadal variation in wind power as high as 10%. The earlier study of Coelingh *et al.* (1998) compared coastal observations to those from surface stations located on three different offshore platforms in the North Sea, finding a daytime peak in surface wind speeds between 1200 and 1400 UTC at the coastal stations, but hardly any diurnal variation at the offshore platforms. Further results from Coelingh *et al.* (1998) highlighted that winds with fetch over the sea presented similar distributions of wind speed with wind direction (aggregated by 12 different sectors) at coastal stations and offshore platforms, as expected given that in both cases the wind fetch stretches over hundreds of km of sea surface (excluding the southerly winds which were shielded at the coastal stations). The link between synoptic-scale flow in intense midlatitude cyclones and associated extreme ocean wave heights has been explored either by looking at individual case study hindcasts (Cardone *et al.*, 2014; Pinto *et al.*, 2014) or by analysing

historical series of extreme wind speeds and ocean wave heights for a selected surface observation station, the Forties oil platform in the North Sea (Bell *et al.*, 2017). The latter study demonstrated that the largest measured wave heights were associated with northwesterly cyclone wind events aided in growth by the large fetch over the central North Sea, but southerly cyclone wind events were found to create large wave heights despite the limited fetch.

In this study, we explore the systematic link between the conveyor belt jets in midlatitude cyclones and observed extreme wind speeds, gusts, and wave heights for the seas surrounding the British Isles. Towards this aim, a climatological analysis has been performed using the 2012–2020 timeseries of extreme wind speeds, gusts, and wave heights observed at 26 stations spread across the seas surrounding the British Isles and then the observed extremes objectively attributed using an algorithm to midlatitude cyclone conveyor belt wind jets. The attribution algorithm detects the frontal boundary between the cyclone cold and warm sectors and then uses the observed surface wind direction to distinguish between the WCB, CCBa, and CCBb jets. Using this partitioning we have quantified the absolute and relative 2012–2020 compound wind-wave risk and ranked the jets accordingly. Finally, we have determined the relationship between the boundary-layer height diagnosed in ERA5 and the jet type, and analysed the ERA5 biases in wind speeds, gusts, and wave heights associated with each jet. We expect that the results of this study could contribute to more accurate estimation of wind power resources and compound wind-wave hazards, and so benefit offshore economic actors.

The remainder of the paper is structured as follows. Section 2 describes the marine observations, reanalysis data, and jet attribution algorithm used. Results are given in section 3, where we show the prevailing wind direction of the extreme wind speeds across the selected marine observation stations along with an analysis of their inter- and intra-annual variability. We also determine at each station whether the WCB, CCBa, or CCBb jet is more likely to lead to an extreme wind speed event, and then discuss the associated flow characteristics and compound wind-wave hazards. Finally, we present the partitioning of ERA5 bias according to the jets. Further discussion and conclusions are given in section 4.

2 | DATA AND METHODS

2.1 | Observations of wind, maximum gust, and wind-wave heights

We analysed hourly reported 10-m wind speeds, direction, wind-wave height (waves still under the action of the winds that created them, rather than free waves such as swells), and hourly or 6-hourly maximum 10-m wind gusts (depending on availability), observed by ship, buoy (for most of the sites), and fixed platform surface stations. The observations from these stations are reported in the SHIP synop code and archived by the Met Office MetDB System at CEDA (Met Office, 2008). The station buoy identification numbers, or call signs for ships and fixed offshore platforms, are provided as Supporting Information. The analysed time period was the 9-year period 2012–2020 (inclusive), selected because it was the longest period for which surface observation data were available in all the North Atlantic Ocean seas surrounding the British Isles considered in this study: the Celtic Sea, the English Channel, and the southern, central, and northern North Sea. The 10-m wind speeds are reported hourly to the nearest 0.1 $m \cdot s^{-1}$ and 10° by all observation stations, while maximum gusts are reported hourly or 6-hourly, depending on the specific station. The hourly 10-m wind speed is measured by averaging the wind fluctuations (sampled every 0.25 s due to their turbulent nature) over the 10-min period leading up to the hourly reporting time. The maximum 10-m gust is the maximum 3-s average wind speed recorded over the full time period leading up to the reporting time (i.e., 1 or 6 hr). Finally, the wind-wave heights are measured hourly and to the nearest 0.1 m.

All the observations considered in this study have passed the rigorous quality control by the Met Office via checks on the equipment and raw data (Met Office, 2008; Hewston and Dorling, 2011). The dataset was further filtered to guarantee a good temporal coverage of the 2012–2020 period. First, we discarded the stations for which more than 10% of the 10-m wind speed measurements were missing (discarding 25, though mostly located in the central and northern North Sea where a dense network of stations was available), obtaining a network of 26 stations which were labelled from A to Z (see map in Figure 2a). Then, for each station we discarded the maximum gusts and wind-wave height timeseries with reports for fewer than 50 and 10%, respectively, of the times available. A less strict threshold was used for the gusts because of the dearth of gust measurements over the seas. At the end of the filtering process, of the 26 stations reporting 10-m wind, 22 also report wind-wave heights, and 10 also report maximum gusts (7-hourly and three 6-hourly), as shown in Figure 2a.

2.2 | Characterization of the extreme tail of the observed wind speeds

In the literature, extreme wind speeds are typically defined as exceeding an upper percentile of wind speed and so

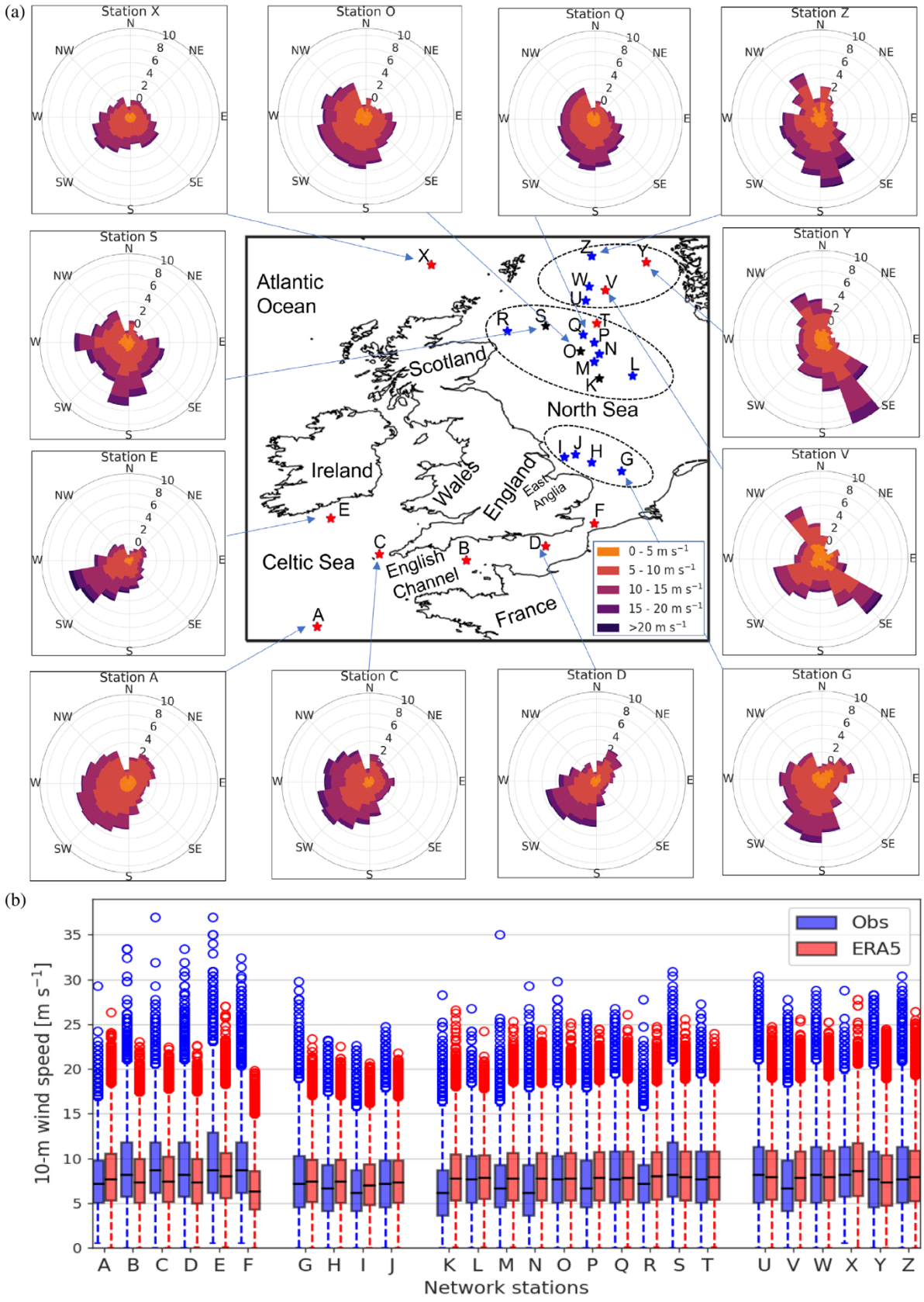

FIGURE 2 Legend on next page.

characterize the upper (or extreme) tail of the wind speed distribution at a given observation station or over a given geographical region (e.g., Hewston and Dorling, 2011; Earl and Dorling, 2013; Earl *et al.*, 2017). Here, we define extreme daily maximum wind speeds as those exceeding the 20 or 25 $m \cdot s^{-1}$ threshold. The 20 $m \cdot s^{-1}$ threshold corresponds to a Beaufort scale of 8 (strong gale), which, over the sea, is associated with moderately high waves with their crests beginning to topple, tumble and roll over, and probable maximum wave heights of up to 7 m (WMO, 1970). Note, however, that 7 m can be considered quite an extreme wind-wave height. For example, as shown by Valiente *et al.* (2021), the wind-wave heights associated with midlatitude cyclone Xaver (December 2013), one of the storms that crossed the UK during the 2013–2014 winter (one of the stormiest winters over northwest Europe in the past few decades), barely exceeded the 7 m threshold in the North Sea regions where the in-situ observation stations used in this paper are located. The 25 $m \cdot s^{-1}$ threshold corresponds to the important operational value of power cut-out because wind turbines can be forced to shut down for wind speeds exceeding this threshold to avoid damage from further operation (Dupont *et al.*, 2018; IMAREST, 2018). However, surface stations report wind speeds at, or corrected to, 10-m height, but the hub height of offshore wind turbines is typically 100–200 m and other offshore installations are also typically taller than 10 m. Hence, in section 3.1 the relationship between 10- and 100-m wind speeds is explored by exploiting the availability of both fields in ERA5. Finally, we define a compound wind-wave hazard, relevant for power cut-out, as the simultaneous occurrence of a 10-m wind speed exceeding 25 $m \cdot s^{-1}$ and significant wind-wave height exceeding 7 m, since, as discussed, extreme wind and waves exceeding these thresholds can damage the offshore infrastructure (PAFA Consulting Engineers, 2001; IMAREST, 2018).

To select only independent extreme wind speed events at each network station, we consider daily maximum wind speed (DMWS), that is, the strongest wind speed reported between 0000–2359 UTC each day, and define a DMWS event if this exceeds the 20 or 25 $m \cdot s^{-1}$ threshold. Moreover, wind directions, gusts, and wind-wave heights associated with the DMWS events (i.e., at the same time as the DMWS) are used to better characterize the atmospheric flow and sea state. For the three stations for which the maximum gust is reported 6-hourly, the gust associated with the event is that at the nearest reporting time ahead of the DMWS time.

2.3 | ERA5 data

ERA5 is the fifth generation hourly reanalysis of the ECMWF (Hersbach *et al.*, 2020). It provides values for atmosphere, ocean, wave, and land surface variables with a horizontal grid resolution of 0.25°, corresponding to $\simeq$ 31 km. The atmospheric component is interpolated to 37 pressure levels from the surface up to 1 Pa. Observations are assimilated in ERA5 from many satellite and conventional surface stations instruments. As detailed in Hersbach *et al.* (2020), because the 10-m wind speed observations we consider are encoded in SHIP SYNOP messages they ought to have been assimilated in ERA5, while wind-wave heights and maximum gusts are not (more details in Hersbach *et al.*, 2020). Although wind-wave heights measured by conventional in situ observations are not assimilated in ERA5, significant wave heights remotely sensed by satellite altimeters are assimilated (Hersbach *et al.*, 2020).

We extracted from ERA5 the following fields: the horizontal components of 10-m wind, 10-m wind direction, and 10-m maximum gust since previous postprocessing, along with wind-wave height, boundary-layer depth, and 850-hPa relative vorticity, ξ_{850}, temperature, and relative humidity. To select the ERA5 data corresponding to each observation station, we extracted the temporal time series of the nearest-neighbour ERA5 grid point. Although it could occur that this method attributes the same ERA5 grid points to different stations, this did not happen in our study.

It is important to note that we compared the observed maximum gust and wind-wave height observations with the corresponding ERA5 fields defined in the same way

FIGURE 2 (a) Map of 10-m wind speed, wind-wave height, and maximum gust observation stations for the 2012–2020 time period, surrounded by wind roses for a set of 12 representative stations showing wind speed distribution per wind direction sector (of 20° width each). The 26 stations are labelled with letters from A to Z, following an order of increasing latitude. Stations are marked with a black star, blue star, or red star according to whether they report 10-m wind speed, 10-m wind speed and wind-wave height, and 10-m wind speed, wind-wave heights, and gust speeds, respectively. The three dashed circles illustrate the cluster of stations in the northern, central, and southern North Sea. (b) Box and whisker plot of observed (blue) and corresponding ERA5 (red) 10-m wind speed at each station. The minimum and maximum values (within 3σ from the mean) are indicated by the ends of the whiskers, with the median, 25th and 75th percentile values marked by the middle, lower and upper parts of the box, respectively

as for the network stations. Thus, the observed maximum gust was compared with ERA5 10-m maximum gust, F_{gust}, which is computed based on the argument that the difference between F_{gust} and the mean 10-m wind speed, F_{10}, is proportional to the standard deviation of the horizontal wind, σ_u. The value of σ_u is computed following the similarity relation of Panofsky *et al.* (1977),

$$\sigma_u = \begin{cases} 2.29u_* \left(1 - \frac{0.5z_{\text{blh}}}{12L}\right)^{\frac{1}{3}} & L<0 \\ 2.29u_* & L>0 \end{cases},$$

where u_* is the friction velocity, z_{blh} the boundary-layer height, L the Monin–Obukhov length, and $L<0$ indicates an unstable boundary layer, while $L>0$ indicates a stable boundary layer. Then, F_{gust} is computed as

$$F_{\text{gust}} = F_{10} + c_{\text{ugn}} u_* f(z_i/L), \quad (1)$$

where z_i is a scale height of the boundary-layer depth and $c_{\text{ugn}} = 7.71$ is a dimensionless number determined from the universal turbulence spectra for a 50% exceeding probability of the three-second wind gust (Beljaars, 1987). The value of F_{gust} every time step, and its maximum value since previous post-processing is output. To account for the effect of deep convection on F_{gust}, in strong convective events a convective contribution as a function of the vertical wind shear is added to Equation (1), which becomes

$$F_{\text{gust}} = F_{10} + c_{\text{ugn}} u_* f(z_i/L) + C_{\text{conv}} \max(0, U_{850} - U_{950}), \quad (2)$$

where C_{conv} is the convective mixing parameter, set to $C_{\text{conv}} = 0.6$, and U_{850} and U_{950} are the wind speeds at 850 and 950 hPa, respectively.

2.4 | Attribution of DMWS events to conveyor belt jets

To determine which conveyor belt jet (WCB, CCBa, and CCBb) each DMWS event (with winds exceeding 20 or 25 $\text{m}\cdot\text{s}^{-1}$) is attributed to, the algorithm outlined below was followed.

1. Calculate the cyclone tracks in the Northern Hemisphere using the TRACK algorithm (Hodges, 1995; Hodges *et al.*, 2011) applied to hourly relative vorticity at 850 hPa, ξ_{850}, smoothed to spectral T63 resolution. Relative vorticity at 850 hPa is a more useful field than mean sea level pressure as it allows cyclone systems to be identified earlier and is also less sensitive to the large scale background, while the spectral filtering to T63 is needed to reduce the noise in what is an otherwise noisy field for the purpose of tracking.
2. For every DMWS event, determine, within a 1,000-km radius, the nearest midlatitude cyclone track point defined by the mean sea level pressure minimum and matching the same time (to the hour) of the observed DMWS event. If a cyclone track point like this exists, the event is classified as "cyclone-associated" (found to be true for $\approx 85\%$ and 90% of events for 20 and 25 $\text{m}\cdot\text{s}^{-1}$ thresholds, respectively).
3. For each "cyclone-associated" DMWS event, compute the 850-hPa equivalent potential temperature, θ_{e850}, representative of the cyclone frontal boundary, defined as $\widetilde{\theta}_{e850}$. Following the methodology of Hart *et al.* (2017), $\widetilde{\theta}_{e850}$ is the mean θ_{e850}, obtained from the ERA5 grid points exceeding the 99th percentile of the gradient of θ_{e850}, $\nabla\theta_{e850}$, within 750 km of the cyclone centre. As in Manning *et al.* (2022), grid points at elevations above 500 m are masked before calculating the 99th percentile of $\nabla\theta_{e850}$ to remove noise introduced by orography.
4. Attribute the "cyclone-associated" DMWS events to the cyclone cold or warm sector by comparing the nearest grid point θ_{e850} with $\widetilde{\theta}_{e850}$. Thus, a "cyclone-associated" DMWS is attributed to the cold sector if $\theta_{e850} < \widetilde{\theta}_{e850}$ and to the warm sector if $\theta_{e850} > \widetilde{\theta}_{e850}$.
5. Further partition the cold and warm sector DMWS events according to the DMWS wind direction α, in the following way:

- A cold sector DMWS event is attributed to the CCBa jet if it has a southeasterly wind direction ($90° \leq \alpha \leq 210°$).
- A cold sector DMWS event is attributed to the CCBb jet if it has a northwesterly wind direction ($240° \leq \alpha \leq 360°$).
- A warm sector DMWS event is attributed to the WCB jet if it has a wind direction ranging from southeasterly to southwesterly ($130° \leq \alpha \leq 250°$).
- All the cold and warm sector DMWS events that have not been attributed to any of the conveyor belt jets are labelled as "other."

This classification method attributes DMWS events to midlatitude cyclone early CCBs (CCBa), returning CCBs (CCBb), or WCBs. As can be seen in Figure 1b, the strong winds associated with the WCB jet lie almost entirely within the warm sector delimited by calculated frontal boundary. It is likely that some of the DMWS events classified as "other" correspond to other causes of strong 10-m winds in cyclones such as convective lines, quasi-convective lines, and embedded frontal convection. Also,

some of the events attributed to the CCBb jet could actually be associated with a SJ as this feature occurs in the same part of the cyclone as the CCBb (when it occurs). However, all these features are too fine scale to be represented by the (relatively) coarse $\simeq 31$ km resolution of the model used to generate ERA5.

3 | RESULTS

3.1 | Wind speed variability over the British Isles surrounding seas

The geographic variability of the observed 10-m wind speeds and directions for the period 2012–2020 is shown in Figure 2a,b, along with the map of the location of the 26 network stations. In Figure 2a, a sample of 12 wind roses illustrates the prevailing wind direction across the network stations, which is overall dominated by the westerly sector of the compass. However, some variations in the wind speed direction occur with latitude, longitude, and distance from the British Isles coasts. The winds for the more southerly stations (A–G) are mainly dominated by the southwestern quadrant, and less so by the northwestern quadrant. In comparison, the central (K–T) and northern North Sea stations (U–Z) generally show less dominance of the southwestern quadrant. For the three northern North Sea stations (V, Y, and Z), the contributions of the northwestern and southeastern quadrants of the compass strongly exceed that of the southwestern quadrant. When considering only 10-m wind speeds exceeding 25 $m{\cdot}s^{-1}$, a similar pattern is revealed (not shown). The predominant southeasterly and northwesterly wind directions in the northern (and less so central) North Sea stations suggest a more important role of the CCBa and CCBb in producing strong surface winds here than for the rest of the network stations. Indeed, due to their geographic location, the central and northern North Sea stations are exposed to more mature midlatitude cyclones in which the CCB has had time to develop (eroding the warm sector). However, the large number of westerly/southwesterly wind events exceeding 20 $m{\cdot}s^{-1}$ at the more southerly stations could also indicate that the CCBb plays an important role in generating gale-force surface winds in this region. In section 3.3 the method presented in section 2 is used to distinguish the different conveyor belt jets.

To better characterize the 10-m wind speed variability at each network station, we plotted the median, quartiles, and extremes of the 10-m wind speed distribution observed at each station along with the corresponding ERA5 values (see Figure 2b). The strongest wind speeds are 37.5 $m{\cdot}s^{-1}$ at stations C (off Cornwall, at the tip of England's southwest peninsula) and E (Celtic Sea, south of Ireland), followed by station M (central North Sea, 35.1 $m{\cdot}s^{-1}$). Station B (English Channel) and stations S, U, and Z (central and northern North Sea) also occasionally report 10-m wind speeds exceeding 30 $m{\cdot}s^{-1}$, but below 35 $m{\cdot}s^{-1}$. The median of the observed 10-m wind speed distribution at each station varies between ≈ 6 and ≈ 9 $m \cdot s^{-1}$. Stations B, D, and F located in the English Channel are characterized by median and upper/lower quartiles ≈ 1.5 $m \cdot s^{-1}$ higher than those of the southern North Sea stations (G–I), but in line with the median of the distribution reported by the central North Sea stations.

Figure 3 shows the number of exceedences in the observations and ERA5 data for both thresholds and for each station per year. The northern North Sea and western English Channel stations experience more wind speed events exceeding the 20 and 25 $m{\cdot}s^{-1}$ thresholds per year than those in the southern/central North Sea, besides presenting higher median and quartile values. For example, station E, in the Celtic Sea immediately south of Ireland, experiences ≈210 wind speed events exceeding 20 $m{\cdot}s^{-1}$ and ≈33 events exceeding 25 $m{\cdot}s^{-1}$, the largest number of exceedances per year of the two wind speed thresholds across all the network stations. The other stations in the Atlantic Ocean, English channel and northern North Sea exceed the thresholds $\approx 50\%$ less often than station E, and even fewer exceedances are observed at the stations in the central North Sea and off the coast of East Anglia (in the southern North Sea). In particular, the stations H–J off East Anglia report between 20 and 50 exceedances of the 20 $m{\cdot}s^{-1}$ threshold and between 0 and 3 exceedances of the 25 $m{\cdot}s^{-1}$ threshold per year, the fewest among the stations.

The variability of the ERA5 10-m wind speed distribution across the stations mirrors that of the observed distributions, as shown in Figure 2b. However, non-negligible differences can be noted in the median, quartiles and also extremes of the ERA5 and observed distributions for several stations. The largest negative biases between the median and the upper/lower quartiles of the ERA5 and observed 10-m wind speed distributions can be seen in the Celtic Sea and English Channel stations B–F, for which ERA5 underestimates the observed median and quartiles by up to ≈ 2 $m \cdot s^{-1}$. Instead, ERA5 overestimates median and quartiles by up to ≈ 2 $m \cdot s^{-1}$ for some of the stations off East Anglia in the southern North Sea (for instance, see stations H and I), and for some of the stations in the central and northern North Sea (for instance, see stations M, N, P, R, and V), with negligible differences ≤ 0.5 $m \cdot s^{-1}$ found for the other stations. The differences between ERA5 and observed winds have a symmetrical distribution for the low to moderate

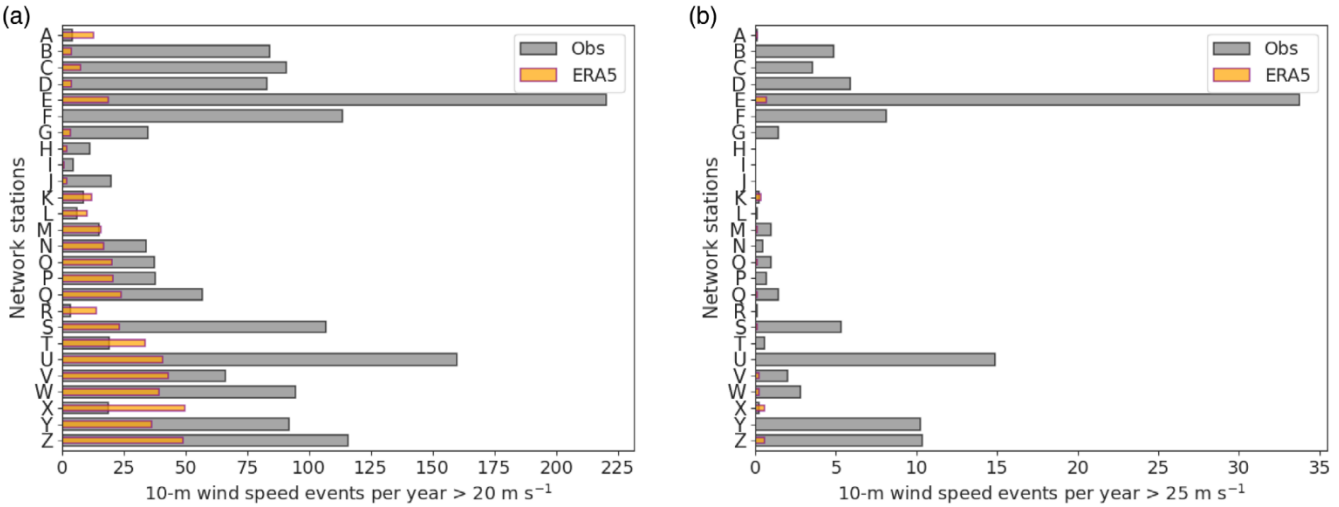

FIGURE 3 Bar chart showing, at each network station, the number of observed (grey) and ERA5 (orange) (a) 20 $m{\cdot}s^{-1}$ and (b) 25 $m{\cdot}s^{-1}$ threshold exceedances of 10-m wind speed events per year

wind speed values (2–20 $m{\cdot}s^{-1}$ range), but consistently smaller ERA5 values for wind speeds exceeding the 20 $m{\cdot}s^{-1}$ threshold, and even more so for those exceeding the 25 $m{\cdot}s^{-1}$ threshold.

Further comparison of observed and ERA5 10-m wind speeds considering the number of exceedances per year of the 20 $m{\cdot}s^{-1}$ threshold shows that the ERA5 exceedances drop to between half and one third of those observed for most of the stations (Figure 3a). The reduced magnitude of the ERA5 wind speeds compared to observed values is even more accentuated for station E, just south of Ireland, which is the only station to report a 10-fold reduction in 20 $m{\cdot}s^{-1}$ threshold exceedances. Considering the higher threshold of 25 $m{\cdot}s^{-1}$, only 10 out of the 26 network stations report ERA5 wind speed exceedances (Figure 3b). Station E reports the largest number of ERA5 exceedances (six), followed by X and Z with five each. In general, the number of observed 25 $m{\cdot}s^{-1}$ exceedances per year is disproportionately higher than for the ERA5 (up to 20 times as higher). However, for station T and X the ERA5 and observed wind speeds exceedances of the 25 $m{\cdot}s^{-1}$ threshold are similar. Apart from these two stations, the ERA5 underestimates the exceedences over the Celtic Sea, the English Channel, and the North Sea. In summary, the higher the observed 10-m wind speed, the more likely it is that the corresponding speed from the ERA5 will have a negative bias. These results confirm and extend previous findings of Molina *et al.* (2021) that indicated that European land stations reporting more frequent exceedances of the 25 $m{\cdot}s^{-1}$ threshold (the only threshold used) were generally associated with larger negative bias in the ERA5.

To investigate how the wind speeds at 10 m height compare to those at 100 m height (approximately the height of offshore wind turbine hubs), a scatterplot considering all the 10- and 100-m ERA5 wind speed data corresponding to the observed 10-m wind speed events by the network stations is shown in Figure 4. This figure shows a roughly linear dependence of the ERA5 100-m wind speeds on the ERA5 10-m wind speeds, modelled by the linear relationship $y=1.23x$, with an excellent R^2 fit of $R^2=0.97$. As can be seen from Figure 4, for 10-m wind speeds above 20 $m{\cdot}s^{-1}$, the dependence of 100-m wind speeds on the 10-m wind speeds becomes slightly steeper, giving 100-m wind speeds which are $\approx 25\%$ larger in value than the corresponding 10-m wind speeds. As a result, an ERA5 10-m wind speed of 20 $m{\cdot}s^{-1}$ corresponds to an ERA5 100-m wind speed close to or above the power cut-out threshold of 25 $m{\cdot}s^{-1}$, highlighting the importance of considering both the 20 and 25 $m{\cdot}s^{-1}$ thresholds for 10-m wind speeds in this study. A similar relationship between ERA5 wind speeds at 10 and 100 m height was also found by Sun *et al.* (2021) for sites located in the Po valley, Italy (though associated with a slightly steeper slope of 1.3).

3.2 | Interannual and monthly variability of wind speeds over the British Isles seas

To characterize the interannual and monthly variability of extreme wind speed events over the British Isles surrounding seas the number of 10-m wind speed exceedances of the two thresholds, 20 and 25 $m{\cdot}s^{-1}$, are aggregated over each station by year in Figure 5a and by month in Figure 5b. Overlain on the intra-annual variability plot is the correspondingly averaged monthly

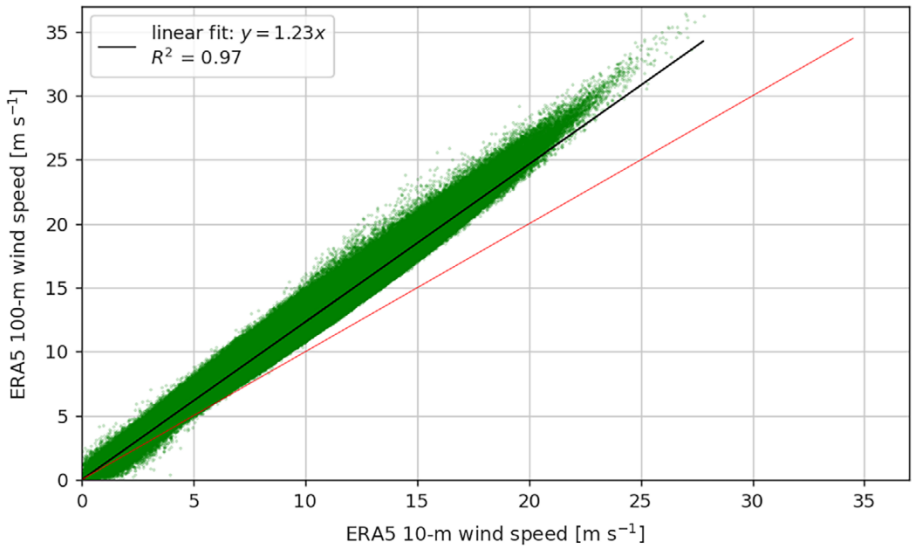

FIGURE 4 Scatterplot of 100-m against 10-m ERA5 wind speeds for all network stations (green scatter points). The black line is the linear fit of the 10-m and 100-m winds while red line is the line of equality. The goodness of the linear fit is given by the R^2 value

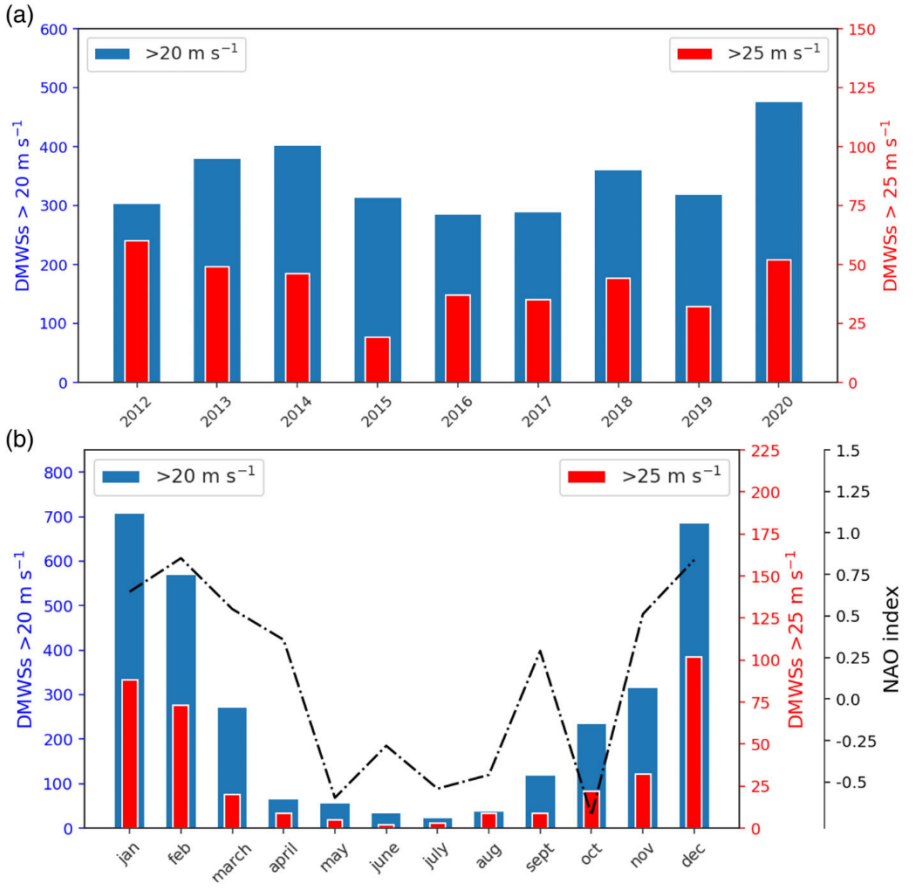

FIGURE 5 (a) Interannual 2012–2020 variability of number of 10-m wind speed events exceeding the 20 and 25 m·s^{-1} threshold, aggregated over all network stations (b) Monthly, intra-annual variability of 10-m wind speeds exceeding the 20 and 25 m·s^{-1} thresholds, aggregated over all network stations, and overlaid by the averages for each month of the 2012–2020 NAO index calculated from the monthly averages produced by the Climate Prediction Center at the National Oceanic Atmospheric Administration (NOAA, 2020)

North Atlantic Oscillation (NAO) index. The NAO is a major mode of wind variability in the Northern Hemisphere and exhibits strong decadal and seasonal variability (Hurrell *et al.*, 2003), the latter evident from Figure 5b.

Figure 5a reveals that the number of exceedances of the 20 m·s^{-1} threshold is typically about 300 events per year for the station network, about 10 times larger than that associated with the 25 m·s^{-1} threshold. Some interannual variability can be observed for the 20 m·s^{-1} threshold exceedances, with the years 2013, 2014, and 2020 presenting the three highest number of exceedances (381, 402, and 477 events, respectively). Indeed, the two midlatitude cyclones that are found to affect all the stations, leading to one of the top five DMWS events (all exceeding 25 m·s^{-1}) recorded by each station, are from

the 2013/2014 and the 2019/2020 cyclone season, respectively, storm Tini, and storm Ciara. However, the interannual variability of the number of 25 $m \cdot s^{-1}$ exceedances does not correlate strongly with that of the 20 $m \cdot s^{-1}$ exceedances. Figure 5b shows that the winter months, December–February, account for ≈80% of the 20 $m \cdot s^{-1}$ threshold exceedances and ≈90% of the 25 $m \cdot s^{-1}$ threshold exceedances. Apart from the NAO index value for September, the monthly NAO index averaged over the 2012–2020 period correlates well with the monthly threshold exceedances, being both highest in the late-autumn and winter months and lowest over spring and summer months. This correlation was expected as a positive NAO index is associated with a stronger North Atlantic jet stream and a northward shift of the storm track leading to northern Europe (including the British Isles) experiencing more cyclones (Hoskins and Hodges, 2019). The relationship between the NAO and midlatitude cyclone characteristics has also been quantified by Rudeva and Simmonds (2015), who found positive correlations between frequency of frontal activity and the NAO in a belt stretching across the North Atlantic to Europe (north of 40°N), with maximum correlation coefficient (exceeding 0.7) east of Newfoundland and over the UK.

In contrast to the obvious relationship between the monthly-averaged NAO index and monthly threshold exceedances shown in Figure 5b, there is no meaningful relationship between the winter-season (or yearly) averaged NAO index for each year and the yearly threshold exceedances plotted in Figure 5a (not shown). This lack of a relationship is consistent with results from recent papers (e.g., Laurila *et al.*, 2021) that show that the correlation between NAO and 10-m wind speeds is not obvious, even on the much longer interdecadal timescales.

3.3 | Climatology of conveyor belt jets contributing to extreme observed 10-m wind speeds

To investigate the attribution of independent extreme wind speed events exceeding the 20 and 25 $m \cdot s^{-1}$ thresholds to cyclone WCB, CCBa, and CCBb jets, DMWS events (computed as the strongest wind speeds observed in the period 0000–2359 UTC each day; for more details; see section 2) are considered. Pie charts in Figure 6a,b summarize the resulting partitioning. Over the 2012–2020 period, the cold sector (which includes CCBa and CCBb jets) accounts for most of the DMWS events with ≈60% of the events exceeding the 20 $m \cdot s^{-1}$ threshold (across all network stations; Figure 6a). This percentage rises to ≈75% of the total events for those exceeding the 25 $m \cdot s^{-1}$ threshold. Considering separately the two CCB jets, the returning CCBb is approximately three times more likely to generate an event exceeding the 20 $m \cdot s^{-1}$ threshold than the early CCBa (16% CCBa vs. 46% CCBb events), and nearly four times more likely to generate an event exceeding the 25 $m \cdot s^{-1}$ threshold (15% of CCBa vs. 59% CCBb events). The CCBb also accounts for the increase in cold sector events between the two thresholds, being associated with 3/5 of the strongest events recorded across the network. In comparison, the WCB accounts only for 25% of the events exceeding the 20 $m \cdot s^{-1}$ threshold and 20% of the events exceeding the 25 $m \cdot s^{-1}$ threshold. Consequently, the CCBb is the most likely conveyor belt to cause strong surface winds across the station network, followed by the WCB and then CCBa. Note that warm or cold sector DMWS events that did not exhibit the wind directions typically associated with conveyor belts in those sectors (S/SW for WCB, W/NW for CCBb, and S/SE for CCBa) were classified as "other" (grey segment in Figure 6a) and represent ≈14% and ≈6% of the total number of events exceeding the 20 and 25 $m \cdot s^{-1}$ thresholds, respectively. An examination of Met Office surface analysis charts for some randomly-picked events labelled as "other," suggested they could plausibly be associated with convective lines, quasi-convective lines, or convective systems in the sectors, but the lack of radar data over the sea and the relatively coarse resolution of ERA5 prohibited their objective classification. Note that, compared to the 20 $m \cdot s^{-1}$ threshold, the contribution of these unidentified conveyor belt wind jet events halved when considering the 25 $m \cdot s^{-1}$ threshold.

The CCBb jet is the dominant conveyor belt jet for DMWS events exceeding both wind thresholds for each cluster of neighbouring stations considered (see Figure 6c) as well as when aggregating over all stations. In contrast, the contribution of the WCB and CCBa jets to events is not homogeneous across the station network. The Celtic Sea, English Channel, and southern North Sea stations are more affected by WCB jets than CCBa jets (with the exception of station C) for both wind speed thresholds. As the latitude and the longitude of the stations increase, the contribution of the CCBa jets becomes larger than WCB jets, with central North Sea and northern North Sea stations exhibiting CCBa events up to twice as often as WCB events (for instance, see northern North Sea 25 $m \cdot s^{-1}$ exceedances in Figure 6c).

3.4 | Flow characteristics of conveyor belt wind jets

The characteristics of the flow associated with each of the conveyor belt jets are depicted in Figure 7a–c for the

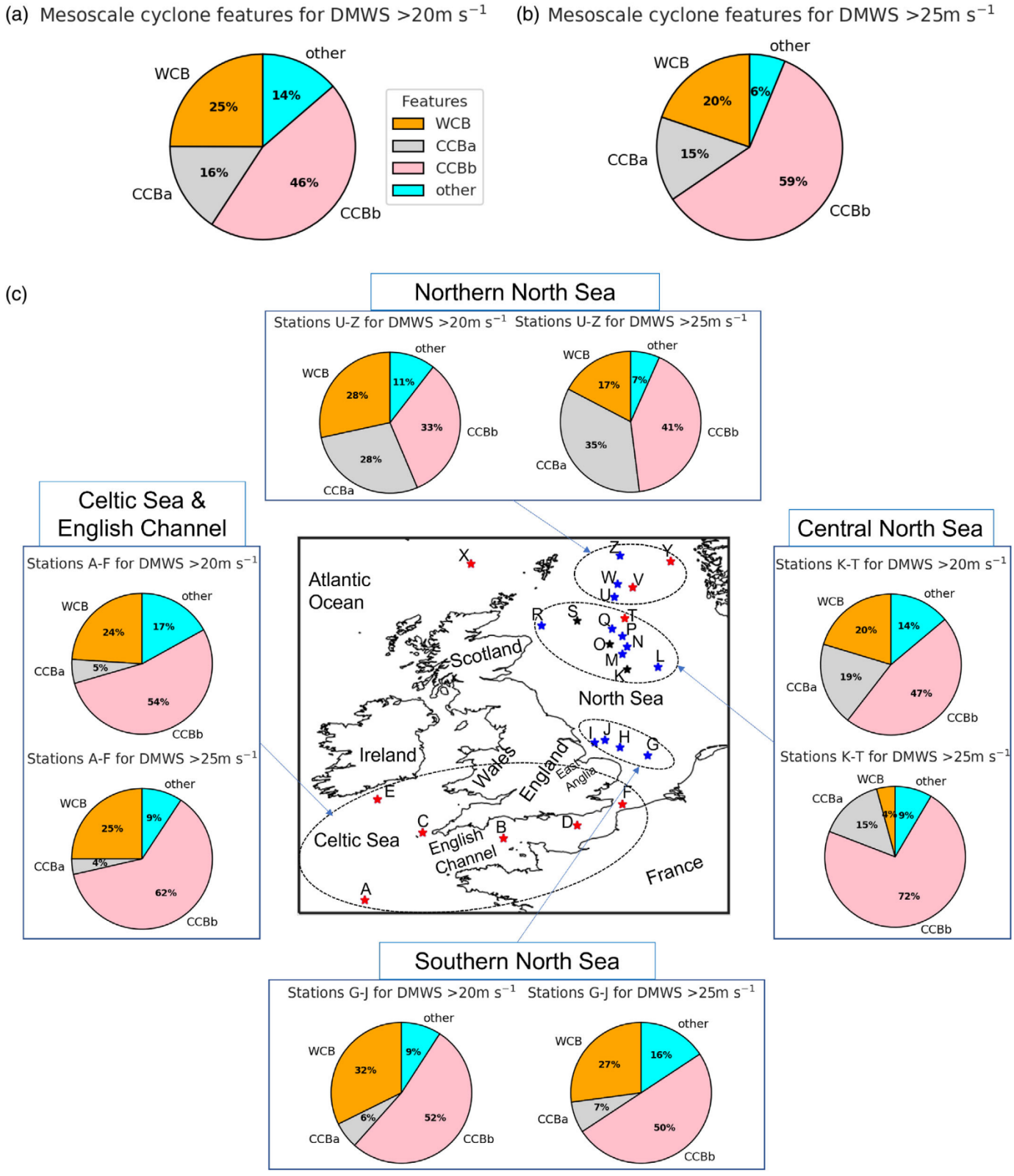

FIGURE 6 Legend on next page.

DMWS events exceeding the 20 and 25 m·s^{-1}. The cold sector winds (associated with CCBa and CCBb) are more intense than the warm sector winds (associated with the WCB) (Figure 7a): the median and the upper quartile of the CCBa and CCBb events exceeding the 20 and 25 m·s^{-1} thresholds are up to 0.5 and 1 m·s^{-1} higher,

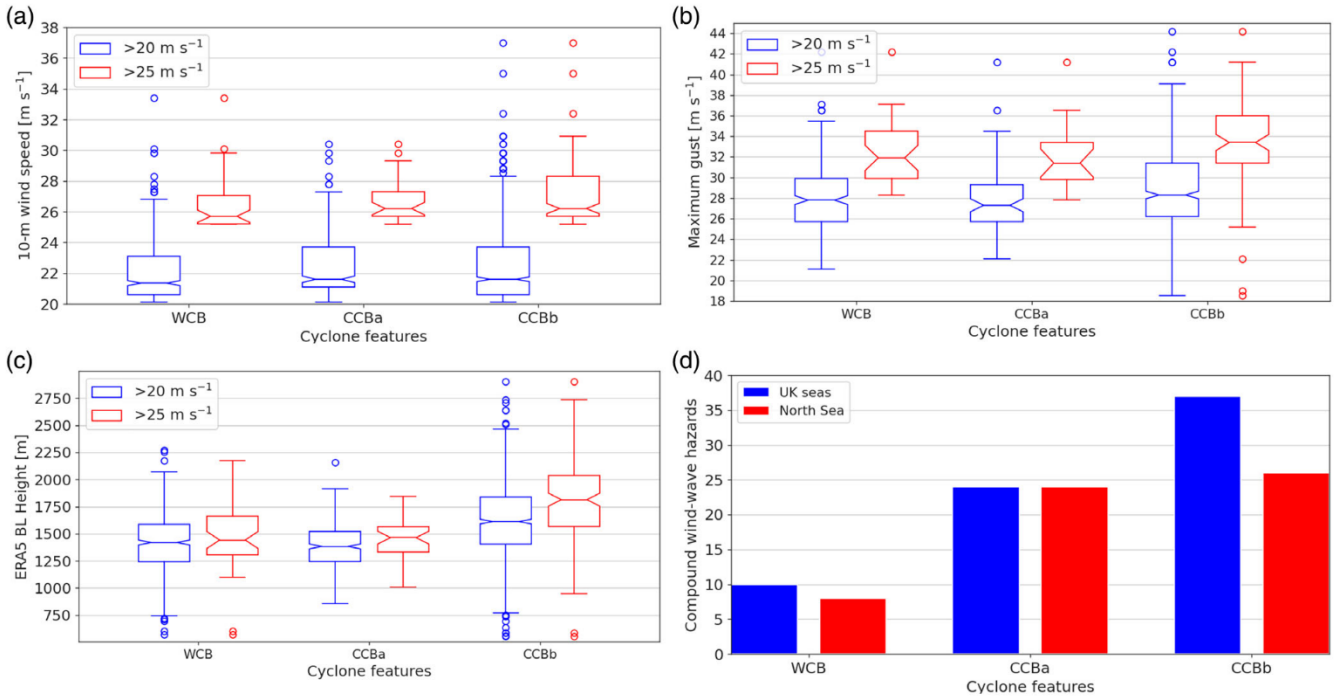

FIGURE 7 Box plot of (a) observed 10-m wind speed, (b) observed gust, and (c) ERA5 boundary-layer height distributions for the WCB, CCBa, and CCBb jets associated with the DMWS events exceeding 20 $m{\cdot}s^{-1}$ (blue) and 25 $m{\cdot}s^{-1}$ (red). Box plots are defined as for Figure 2. (d) Histogram of number of DMWS events exceeding 25 $m{\cdot}s^{-1}$ co-occurring with observed significant wind-wave height events exceeding 7 m height, associated with WCB, CCBa, and CCBb jets. The blue histogram bars show the number of the wind-wave compound events aggregated over all the network stations in the British Isles surrounding seas, while the red histogram bars are for the northern and central North Sea station clusters only

respectively, than the corresponding WCB values. A closer look at the wind speeds exceeding the higher threshold shows that, excluding the outliers of each distribution, the upper tail (whisker) of the CCBb events is the most intense, ranging between 28.2 and 30.8 $m{\cdot}s^{-1}$, but no appreciable difference can be seen between the upper tails for the CCBa and WCB events (both ranging between 27.1 and 29.6 $m{\cdot}s^{-1}$). The gustiness of the conveyor belt wind jet events, shown in Figure 7b, has been derived from the observed gusts associated with the DMWS events (i.e., taking the gust value closest to the time of each DMWS event, as described in section 2.2). The median and upper quartile values of the gusts for the CCBb events (exceeding 20 $m{\cdot}s^{-1}$) are 28.1 and 31.8 $m{\cdot}s^{-1}$, respectively, with extreme values reaching 39.1 $m{\cdot}s^{-1}$ (excluding outliers). The WCB and CCBa median and upper quartile values are smaller than the CCBb ones: 27.8 and 30.2 for the WCB median and upper quartile and 27.3 and 29.3 for the corresponding CCBa values. Both the median and upper quartile of the gusts observed for CCBb, CCBa, and WCB events exceeding the 25 $m{\cdot}s^{-1}$ threshold are ≈5, ≈4, and ≈3 $m{\cdot}s^{-1}$ larger, respectively, than the corresponding 20 $m{\cdot}s^{-1}$ values.

Figure 7c shows that the CCBb events are associated with deeper boundary layers (diagnosed from ERA5) than WCB and CCBa events. The median and upper quartile of the boundary-layer height of the CCBb events exceeding 20 $m{\cdot}s^{-1}$ are ≈200 m higher than those of the WCB events and ≈250 m higher than those of the CCBa events. For the higher 25 $m{\cdot}s^{-1}$ threshold, the CCBb boundary-layer height distribution median and upper quartile are ≈400 m higher than those for the WCB and

FIGURE 6 Pie charts showing the percentage of conveyor belt jets associated with (a) >20 $m{\cdot}s^{-1}$ and (b) >25 $m{\cdot}s^{-1}$ DMWSs, aggregated over all observation stations. (c) Distribution of conveyor belt jets associated with DMWSs aggregated over distinct geographical regions of the British Isles surrounding seas: Celtic Sea and English Channel, southern North Sea, central North Sea, northern North Sea, illustrating how the relative percentage of features vary with latitude and longitude across the network. Orange sector corresponds to WCB events, grey sector to CCBa events, pink to CCBb events, and light blue to DMWSs which could not be associated with any of the cyclone features WCB, CCBa, and CCBb. In total there are 2,267 DMWS events exceeding the 20 $m{\cdot}s^{-1}$ threshold, and 267 DMWS events exceeding the 25 $m{\cdot}s^{-1}$ threshold associated with a midlatitude cyclone track point

CCBa, almost twice as large as those observed for the lower 20 $m \cdot s^{-1}$ threshold. When considering only the CCBb boundary-layer height values lying above the distribution upper quartile, these can reach ≈2750 m, compared to maximum WCB and CCBa values of ≈2200 and ≈1800 m, respectively (excluding outliers). The deeper boundary layers associated with the CCBb jet compared to the WCB and CCBa jets are consistent with expectations for a jet in the cold sector of cyclones (e.g., Sinclair *et al.*, 2010).

Overall, these results indicate that the CCBb is associated with the strongest observed winds, the highest gustiness, and the deepest boundary layers. The WCB and CCBa can also produce very strong winds, but not as strong as those attributed to the CCBb. This is likely influenced somewhat by the instability in the surface layer generated when the cool air of the CCBb hooks around the cyclone pressure low and descends over warmer ocean waters facilitating the downward mixing of fast flowing air from the top of the boundary layer and thus producing stronger and gustier winds, compared to the other cyclone features. Despite slightly stronger winds in the CCBa events, the median of the CCBa gusts is ≈1 $m \cdot s^{-1}$ less intense than for WCB events. A possible explanation is that the typically deeper boundary layer associated with the WCB is more turbulent, leading to enhanced momentum transport towards the surface and consequently stronger gusts.

Figure 7d shows the compound wind-wave hazard reported by the network stations (wind speed exceeding 25 $m \cdot s^{-1}$ co-occurring with wind-wave height exceeding 7 m at the same time as a DMWS event). The CCBb jet is the most hazardous followed by the CCBa jet and then the WCB jet. The network stations reported 37 compound wind-wave hazards associated with the CCBb jet, 24 associated with the CCBa jet, and 10 associated with the WCB jet. Considering the North Sea stations only, the gap between the number of compound wind-wave hazards produced by the CCBb and CCBa jets is even smaller, with the CCBb jet producing only 2 more compound wind-wave hazards, 26, than the CCBa jet, 24. Moreover, Figure 7d shows that the CCBa is more than twice as likely as the WCB jet to produce a compound wind-wave hazard for the full set of network stations and more than three times more likely when considering only the North Sea stations, despite the WCB jet being responsible for 5% more cyclone-associated DMWS events exceeding 25 $m \cdot s^{-1}$ than the CCBa (Figure 6b). Overall, these findings indicate that the most likely wind speed directions for compound wind-wave hazards are westerly/northwesterly flow (associated with the CCBb) followed by the south/southeasterly flow (associated with the CCBa). A plausible explanation for the highest number of compound wind-wave hazards being attributed to the CCBb being is that the long fetch of its intense northwesterly/westerly winds favours the formation of extreme wind-wave heights, as noted by Ponce de León and Guedes Soares (2014), Bell *et al.* (2017), and Ponce de León and Bettencourt (2021). Note that, because the 100-m wind speeds typically exceed those at 10-m (Figure 4 showed that they are ≈25% stronger in ERA5 data) wind turbines are likely to cut-out at 10-m wind speed thresholds weaker than 25 $m \cdot s^{-1}$. Also significant wave heights of around 2 m can be sufficient to inhibit the safe working of associated vessels, far less than the 7 m threshold used here. Hence, this definition of compound wind-wave hazards can be considered extreme.

3.5 | ERA5 bias of the conveyor belt jet winds and waves

The distribution of the bias of the ERA5 10-m winds, gusts, and wind-wave heights associated with the observed WCB, CCBa, CCBb jet events is shown in the box plots in Figure 8. On average the ERA5 underestimates all three fields for the events. The CCBb events have the highest negative bias with a median at −4.6 $m \cdot s^{-1}$, roughly 0.5 $m \cdot s^{-1}$ larger in magnitude than for WCB events and 1.2 $m \cdot s^{-1}$ larger than for CCBa events (Figure 8a). The same pattern occurs for the lower tails (larger negative biases) of the distributions, as defined by the lower whiskers of the box plots, with values reaching −12 $m \cdot s^{-1}$ for CCBb events (though the lower outliers extend to similar values for the WCB and CCBb). The differences between the ERA5 gust bias distributions for each jet event follow a similar pattern to those for the 10-m wind speed biases (Figure 8b): the lower tail of the CCBb events gust bias extends to −20.2 $m \cdot s^{-1}$ (with outliers extending to −23.3 $m \cdot s^{-1}$). As discussed in section 2.2, three stations only report gusts 6-hourly. However, virtually identical median and quartiles were obtained if observations from these stations were excluded (although there were slight changes to the extreme values of gust bias distribution). This similarity implies that the results are robust to the different reporting frequencies.

The distribution of the biases for the WCB events, and more so for the CCBa events, are narrower than the CCBb events for all fields considered, even when considering the outliers. However, while the gust and 10-m wind speed bias distributions of the CCBa and WCB events are characterized by a smaller magnitude medians than for the CCBb events, the CCBa and WCB events wind-wave height bias distributions are characterized by a larger magnitude median than for the CCBb events (−3.4, −2.7, and −2.0 m for CCBa, WCB, and CCBb events, respectively).

To investigate whether the larger absolute errors (relative to observed values) of ERA5 maximum gusts

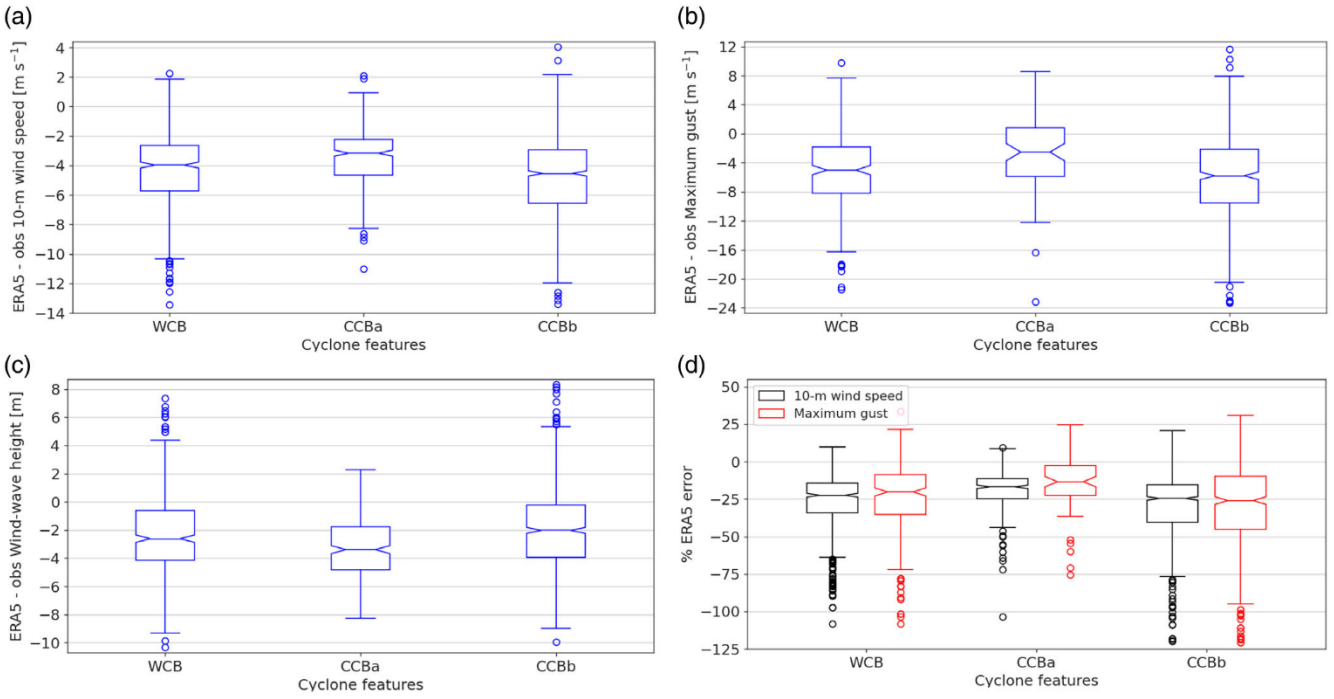

FIGURE 8 (a–c) Box plots showing the bias of ERA5 for (a) 10-m wind speed, (b) gust, and (c) wind-wave heights values of the DMWSs, computed as the difference between ERA5 and observed values and partitioned by the conveyor belt jets (WCB, CCBa, and CCBb). (d) Box plots of the percentage ERA5 error, computed from 100× (ERA5 value-observation)/observation, for each 10-m wind speed (black box plots) and maximum gust (red box plots). Box plots are defined as for Figure 2.

compared to ERA5 10-m wind speeds were simply due to the generally larger wind gust values or instead also corresponded to a proportionally larger error, the percentage error was computed and partitioned per conveyor belt as shown in Figure 8d. For each conveyor belt jet, the median of the ERA5 10-m wind speed percentage error roughly corresponds to that of the maximum gust (within $\approx \pm 2\%$), indicating that the larger absolute errors of the ERA5 maximum gusts do not translate into proportionally higher errors (once normalized by the field value). However, the relative differences between the conveyor belt jets shown in Figure 8a,b are preserved when considering the percentage error. The CCBb jet has the highest negative percentage error in 10-m wind speeds and gusts (medians, respectively, of -25% and -25.5%), followed by the WCB jet (medians, respectively, of -22.5% and -22.6%), and then the CCBa jet (medians, respectively, of -16.3% and -14.4%), mirroring the pattern found for the absolute errors.

4 | DISCUSSION AND CONCLUSION

In this study, a climatology of observed marine extreme wind speeds over the seas surrounding the British Isles has been produced for a 9-year time period (2012–2020) based on a network of 26 stations, and extreme events have been attributed to midlatitude cyclone conveyor belt jets. Extreme DMWS events were defined as occurring for 10-m wind speeds exceeding the 20 and 25 $m \cdot s^{-1}$ thresholds; these two thresholds characterize the extreme tail of the wind speed distribution. The extreme DMWS events were objectively attributed to a cyclone conveyor belt jet (WCB, CCBa, or CCBb) by a two-step algorithm. First, these events are attributed to a cyclone if they occurred within a 1,000-km radius from a midlatitude cyclone track point defined by the mean sea level pressure minimum at a coincident time. Then each event is objectively attributed to a jet based on whether the event is in the cold or warm sector of the cyclone (diagnosed from ERA5 data) and the observed wind direction. We also analysed the distributions of observed gusts and wind-wave heights, and ERA5 boundary-layer heights, associated with each jet event. The climatological compound hazard of each jet was determined by computing the number of DMWS events with wind speeds exceeding 25 $m \cdot s^{-1}$ and co-occurring wind-wave heights exceeding 7 m. Lastly, we calculated the ERA5 bias in the DMWS events associated with the jets to demonstrate the limitations of ERA5 for evaluation of marine wind speeds and the associated gusts and wind-wave heights.

The climatology showed that the winds recorded by the network stations located in the Celtic sea and English Channel were predominantly westerly and southwesterly, consistent with previous extreme wind and gust climatologies over the UK land (Hewston and Dorling, 2011), but stations located in the central North Sea and northern North Sea also recorded pronounced northwesterly and southeasterly wind direction components. The stations in the English Channel and northern North Sea recorded up to 1 $m \cdot s^{-1}$ higher median wind speeds than those in the central and southern North Sea, the latter reporting virtually no exceedances of the higher 25 $m \cdot s^{-1}$ threshold due to sheltering from the nearby land. Comparable differences in magnitude between mean wind speeds in the northern North Sea and central and southern North Sea were also found by Laurila *et al.* (2021) for a longer time period climatology (1979–2018) of wind speeds from the ERA5 over the North Atlantic and European domain.

The DMWS events did not show a clear interannual trend. However, the 2 years that exhibited the most events exceeding the 20 $m \cdot s^{-1}$ threshold (2014 and 2020 with approximately 400 and 500 exceedances, respectively) were also characterized by the most dense midlatitude cyclone seasons, as reported by (Kendon, 2020). When considering the seasonal trend, the winter months (December–February) were the dominant contributors, accounting for 70% and 80% of the extreme wind speeds exceeding the 20 and 25 $m \cdot s^{-1}$ thresholds, respectively; this is consistent with Earl *et al.* (2017) results based on extreme maximum gusts (top 2 and 0.1%) observed by the UK land stations.

Objective attribution, by means of an algorithm, of the extreme DMWS events exceeding the 20 $m \cdot s^{-1}$ threshold (over the period 2012–2020) to the conveyor belt jets demonstrated that the CCBb jet, occurring when the direction of the CCB jet is aligned with the cyclone direction of travel, accounts for most DMWS events (46%), followed by the WCB (25%), and then the early part of the CCB, the CCBa (15%). The CCBb is found to play an even larger role in influencing the DMWS events exceeding the higher 25 $m \cdot s^{-1}$ threshold (59%). In contrast, the role of the WCB is reduced, accounting just for 20% of these events, consistent with results found for cyclone feature association over land (Earl *et al.*, 2017). When considering separately the different regions of the North Atlantic Ocean seas surrounding the British Isles, the CCBb is confirmed as the most dominant feature in all regions, but for the central and northern North Sea regions the CCBa replaces the WCB as the second most dominant jet. Cold sector (CCBa and CCBb) events are three to four times more likely than warm sector (WCB) events for both thresholds considered, and this can be explained by the British Isles being at the end of the North Atlantic storm track (Dacre and Gray, 2009). Because the WCB develops earlier than the CCB in the midlatitude cyclone lifecycle (see fig. 1 in Hewson and Neu, 2015), by the time the cyclones reach the British Isles the warm sector has already been eroded. In fact, the central North Sea stations reported the smallest number of DMWS events associated with the WCB, with these stations being the farthest from the storm tracks reaching the British Isles.

The CCBb jet led to stronger winds at the surface and, during DMWS events, is associated with higher gusts than CCBa and WCB, probably because the CCBb boundary layer is buoyancy driven, as suggested by the deeper CCBb ERA5 boundary-layer heights than the CCBa and WCB jets. The cool air of the CCB, while hooking around the cyclone low-pressure centre and flowing over warmer ocean water, forces large and positive heat fluxes, in addition to the large momentum fluxes associated with wind shear (Sinclair *et al.*, 2010). The resulting unstable and turbulent surface layer facilitates the downward mixing of high momentum air from the boundary-layer top and produces stronger and gustier winds compared to the other jets (Coronel *et al.*, 2016). Instead, the warm air of the WCB, while flowing over the cooler ocean water, forces negative heat fluxes which enhance the static stability of the boundary layer, leading to a more shallow, shear-driven boundary layer, as suggested by the shallower boundary-layer heights than the CCBb events. Lastly, that the CCBa events are characterized by smaller gusts than WCB events despite being associated with larger surface wind speeds can be plausibly explained by the magnitude of the (positive) surface heat fluxes being smaller than on the equatorward flank of the cyclone (where the CCBb occurs), given that in the CCBa (the early part of the CCB) the CCB cool air has not already mixed down to the surface layer.

In addition to being associated with the largest number of extreme DMWSs events, the CCBb jet was also found to be responsible for the largest number of compound wind-wave hazards, followed by the CCBa and then WCB jets. Although the CCBa accounted for fewer events exceeding the 25 $m \cdot s^{-1}$ threshold than the WCB, it led to more than twice the number of compound wind-wave hazards than the WCB, only $\approx 30\%$ less than for the CCBb. When restricting the analysis to the North Sea stations only, the southerly/southeasterly CCBa events were found to cause 24 compound wind-wave hazards, just 2 fewer than those caused by westerly/northwesterly CCBb events. This result extends previous findings of Bell *et al.* (2017) who also found that cyclone-associated southerly winds can create nearly as many large wave heights as northwesterly winds despite their limited fetch

over the North Sea. However, unlike in this paper they did not perform an objective attribution to the conveyor belt jets.

The partitioning of the ERA5 biases showed that the ERA5 typically underestimated the observed extreme wind speeds, gusts and wave heights for all jet events. The extreme winds and gusts were most underestimated for the CCBb events, with median absolute biases of −4.5 and $-5.5\ \mathrm{m\cdot s^{-1}}$, respectively, but approximately equal percentage errors (approximately −25%) due to the larger values of the maximum gusts relative to the 10-m wind speeds. However, the largest underestimate of the wind-wave heights was associated with the CCBa events, with a median absolute bias of −2.88 m. A possible explanation could be that the generation of large wind-waves occurring when the wind has a short fetch (as for the CCBa jet events in the North Sea) is less well represented in ERA5 than when the fetch is longer (as for the CCBb jet events, associated with the smallest bias). As the resolution of ERA5 is insufficient to represent mesoscale extratropical cyclone processes associated with strong winds and gusts at the surface such as SJs and convective lines, it was not possible to attribute extreme DMWS events to these and other mesoscale features. The SJ precursor tool developed by Martínez-Alvarado *et al.* (2012) could be used to determine the likelihood that some of the events attributed to the CCBb by the ad hoc algorithm developed here are instead associated with SJs. By combining the attribution algorithm with the SJ precursor tool, it would be possible to obtain both an estimate of the ERA5 bias associated with the SJ and a more accurate estimate of the ERA5 bias associated with the CCBb. In addition, the recent availability of new high resolution re-analysis and other products providing wind speeds over decadal periods with hourly or subhourly temporal frequency could form the basis of further future research on attribution of extreme wind speeds to mesoscale extratropical cyclone features. Examples of these products are the recently developed Copernicus European Regional Reanalysis (CERRA) and the New European Wind Atlas (mesoscale dataset) with 5.5 km and 3 km grid spacing, respectively.

Overall, our results reveal that hazardous marine wind (both 10-m wind and gust) and compound wind-wave events near the British Isles are most commonly associated with the CCBb jet that occurs when the CCB hooks around the low-pressure cyclone centre into the southwest quadrant of a mature cyclone. However, the CCBa jet can be nearly as hazardous when considering compound wind-wave events, especially in the North Sea with 24 CCBa events over the 9 years analysed compared to 26 CCBb events. Hence, accurate simulation of these cyclone conveyor belt jets is critical for assessment of marine hazards in both weather forecasts and climate integrations.

AUTHOR CONTRIBUTIONS

Emanuele S. Gentile: Conceptualization; investigation; writing – original draft; methodology; validation; visualization; writing – review and editing; software; formal analysis; data curation. **Suzanne L. Gray:** Conceptualization; funding acquisition; methodology; writing – review and editing; formal analysis; project administration; resources; supervision.

ACKNOWLEDGEMENTS

We are grateful to Dr. Kevin Hodges (University of Reading) for provision of the cyclone tracking algorithm and support for its use in the algorithm developed and used in this paper. Emanuele S. Gentile's contribution was funded through a Natural Environment Research Council (NERC) Industrial CASE studentship in collaboration with the Met Office (NE/R007640/1).

CONFLICT OF INTEREST

The authors declare no potential conflict of interest.

DATA AVAILABILITY STATEMENT

The ERA5 dataset is publicly available and Global Marine Meteorological Observations data is available upon request to CEDA (Met Office, 2008).

REFERENCES

Beljaars, A. (1987) The influence of sampling and filtering on measured wind gusts. *Journal of Atmospheric and Oceanic Technology*, 4, 613–626.

Bell, R., Gray, S. and Jones, O. (2017) North Atlantic storm driving of extreme wave heights in the North Sea. *Geophysical Research Letters*, 122, 3253–3268.

Bourassa, M.A., Meissner, T., Cerovecki, I., Chang, P.S., Dong, X., De Chiara, G., Donlon, C., Dukhovskoy, D.S., Elya, J., Fore, A., Fewings, M.R., Foster, R.C., Gille, S.T., Haus, B.K., Hristova-Veleva, S., Holbach, H.M., Jelenak, Z., Knaff, J.A., Kranz, S.A., Manaster, A., Mazloff, M., Mears, C., Mouche, A., Portabella, M., Reul, N., Ricciardulli, L., Rodriguez, E., Sampson, C., Solis, D., Stoffelen, A., Stukel, M.R., Stiles, B., Weissman, D. and Wentz, F. (2019) Remotely sensed winds and wind stresses for marine forecasting and ocean modeling. *Frontiers in Marine Science*, 6, 1–28.

Browning, K.A. and Roberts, N.M. (1994) Structure of a frontal cyclone. *Quarterly Journal of the Royal Meteorological Society*, 120, 1535–1557.

Cardone, V., Callahan, B.T., Chen, H., Cox, A.T., Morrone, M.A. and Swail, V.R. (2014) Global distribution and risk to shipping of very extreme sea states (VESS). *International Journal of Climatology*, 35, 69–84.

Catto, J., Madonna, E., Joos, H., Rudeva, I. and Simmonds, I. (2015) Global relationship between fronts and warm conveyor belts

and the impact on extreme precipitation. *Journal of Climate*, 28, 8411–8429.

Catto, J. and Raveh-Rubin, S. (2019) Climatology and dynamics of the link between dry intrusions and cold fronts during winter. Part I: global climatology. *Climate Dynamics*, 53, 1873–1892.

Clark, M. (2013) A provisional climatology of cool-season convective lines in the UK. *Atmospheric Research*, 123, 180–196.

Clark, P.A. and Gray, S.L. (2018) Sting jets in extratropical cyclones: a review. *Quarterly Journal of the Royal Meteorological Society*, 144, 943–969.

Coelingh, J., van Wijk, A. and Holtslag, A. (1998) Analysis of wind speed observations over the North Sea coast. *Journal of Wind Engineering and Industrial Aerodynamics*, 73, 125–144.

Coronel, B., Ricard, D., Rivière, G. and Arbogast, P. (2016) Cold-conveyor-belt jet, sting jet and slantwise circulations in idealized simulations of extratropical cyclones. *Quarterly Journal of the Royal Meteorological Society*, 142, 1781–1796.

Dacre, H. and Gray, S. (2009) The spatial distribution and evolution characteristics of North Atlantic cyclones. *Monthly Weather Review*, 137, 99–115.

Dupont, E., Koppelaar, R. and Jeanmart, H. (2018) Global available wind energy with physical and energy return on investment constraints. *Applied Energy*, 209, 322–338.

Earl, N. and Dorling, S. (2013) 1980–2010 variability in U.K. surface wind climate. *Journal of Climate*, 26, 1172–1191.

Earl, N., Dorling, S., Starks, M. and Finch, R. (2017) Subsynoptic-scale features associated with extreme surface gusts in UK extratropical cyclone events. *Geophysical Research Letters*, 44, 3932–3940.

Eisenstein, L., Schulz, B., Qadir, G.A., Pinto, J.G. and Knippertz, P. (2022) Objective identification of high-wind features within extratropical cyclones using a probabilistic random forest (RAMEFI). Part I: method and illustrative case studies. *Weather and Climate Dynamics Discussions*, 3, 1157–1182.

Geyer, B., Bisling, P. and Winterfeldt, J. (2015) Climatology of North Sea wind energy derived from a model hindcast for 1958–2012. *Journal of Wind Engineering and Industrial Aerodynamics*, 147, 18–29.

Hart, N.C.G., Gray, S.L. and Clark, P.A. (2017) Sting-jet windstorms over the North Atlantic: climatology and contribution to extreme wind risk. *Journal of Climate*, 30, 5455–5471.

Hersbach, H., Bell, B., Berrisford, P., Hirahara, S., Horányi, A., Muñoz-Sabater, J., Nicolas, J., Peubey, C., Radu, R., Schepers, D., Simmons, A., Soci, C., Abdalla, S., Abellan, X., Balsamo, G., Bechtold, P., Biavati, G., Bidlot, J., Bonavita, M., De Chiara, G., Dahlgren, P., Dee, D., Diamantakis, M., Dragani, R., Flemming, J., Forbes, R., Fuentes, M., Geer, A., Haimberger, L., Healy, S., Hogan, R., Hólm, E., Janisková, M., Keeley, S., Laloyaux, P., Lopez, P., Lupu, C., Radnoti, G., de Rosnay, P., Rozum, I., Vamborg, F., Villaume, S. and Thépaut, J.-N. (2020) The ERA5 global reanalysis. *Quarterly Journal of the Royal Meteorological Society*, 146, 1999–2049.

Hewson, T.D. and Neu, U. (2015) Cyclones, windstorms and the IMILAST project. *Tellus A*, 67, 27–128.

Hewston, R. and Dorling, S. (2011) An analysis of observed daily maximum wind gusts in the UK. *Journal of Wind Engineering and Industrial Aerodynamics*, 91, 845–856.

Hodges, K.I. (1995) Feature tracking on the unit sphere. *Monthly Weather Review*, 123, 3458–3465.

Hodges, K.I., Lee, R.W. and Bengtsson, L. (2011) A comparison of extratropical cyclones in recent reanalyses ERA-Interim, NASA, MERRA, NCEP, CFSR, and JRA-25. *Journal of Climate*, 24, 4888–4906.

Hoskins, B.J. and Hodges, K.I. (2019) The annual cycle of northern hemisphere storm tracks. Part I: seasons. *Journal of Climate*, 32, 1743–1760.

Hurrell, J.W., Kushnir, Y., Ottersen, G. and Visbeck, M. (2003) *The North Atlantic Oscillation: Climate Significance and Environmental Impact*. Washington D.C.: American Geophysical Union.

IMAREST. (2018) *Metocean procedures guide for offshore renewables*. Available at: https://www.imarest.org/reports/650-metocean-procedures-guide/file.

Kendon, M. (2020) *Met Office report of storm Ciara*. Available at: https://www.metoffice.gov.uk/binaries/content/assets/metofficegovuk/pdf/weather/learn-about/uk-past-events/interesting/2020/2020_02_storm_ciara.pdf.

Laurila, T.K., Sinclair, V.A. and Gregow, H. (2021) Climatology, variability, and trends in near-surface wind speeds over the North Atlantic and Europe during 1979–2018 based on ERA5. *International Journal of Climatology*, 41, 2253–2278.

Madonna, E., Wernli, H., Joos, H. and Martius, O. (2014) Warm conveyor belts in the ERA-Interim dataset (1979–2010). Part I: climatology and potential vorticity evolution. *Journal of Climate*, 27, 3–26.

Manning, C., Kendon, E., Fowler, H., Roberts, N.M., Berthou, S., Suri, D. and Roberts, M. (2022) Extreme windstorms and sting jets in convection-permitting climate simulations over Europe. *Climate Dynamics*, 58, 2387–2404.

Martínez-Alvarado, O., Baker, L.H., Gray, S.L., Methven, J. and Plant, R.S. (2014) Distinguishing the cold conveyor belt and sting jet air streams in an intense extratropical cyclone. *Monthly Weather Review*, 142, 2571–2595.

Martínez-Alvarado, O.S., Gray, S., Catto, J. and Clark, P. (2012) Sting jets in intense winter North-Atlantic windstorms. *Environmental Research Letters*, 7, 1–8.

Met Office. (2008) *Ship SYNOP reports from ship, buoy and fixed platform stations collected by the Met Office MetDB System. NCAS British Atmospheric Data Centre*. Available at: https://catalogue.ceda.ac.uk/uuid/65ca7898647cc3686492bcb8bb483a1cl [Accessed on 10th December 2021].

Molina, M.O., Gutiérrez, C. and Sánchez, E. (2021) Comparison of ERA5 surface wind speed climatologies over Europe with observations from the HadISD dataset. *Quarterly Journal of the Royal Meteorological Society*, 144, 943–969.

Neu, U., Akperov, M.G., Bellenbaum, N., Benestad, R., Blender, R., Caballero, R., Cocozza, A., Dacre, H.F., Feng, Y., Fraedrich, K., Grieger, J., Gulev, S., Hanley, J., Hewson, T., Inatsu, M., Keay, K., Kew, S.F., Kindem, I., Leckebusch, G.C., Liberato, M.L. R., Lionello, P., Mokhov, I.I., Pinto, J.G., Raible, C.C., Reale, M., Rudeva, I., Schuster, M., Simmonds, I., Sinclair, M., Sprenger, M., Tilinina, N.D., Trigo, I.F., Ulbrich, S., Ulbrich, U., Wang, X.L. and Wernli, H. (2013) IMILAST: a community effort to intercompare extratropical cyclone detection and tracking algorithms. *Bulletin of the American Meteorological Society*, 94, 529–547.

NOAA. (2020) *North Atlantic Oscillation (NAO)*. Available at: www.cpc.ncep.noaa.gov/products/precip/CWlink/pna/nao.shtml [Accessed on 30th March 2022].

PAFA Consulting Engineers. (2001) *Weather-sensitive offshore operations and Metocean data*. Available at: https://www.hse.gov.uk/research/otopdf/2001/oto01022.pdf.

Panofsky, H., Tennekes, H., Lenschow, D. and Wyngaard, J. (1977) The characteristics of turbulent velocity components in the surface layer under convective conditions. *Boundary-Layer Meteorology*, 11, 355–361.

Parton, G.A., Dore, A. and Vaughan, G. (2010) A climatology of mid-tropospheric mesoscale strong wind events as observed by the MST radar, Aberystwyth. *Meteorological Applications*, 17, 340–354.

Pinto, J., Gómara, I., Masato, G., Dacre, H.F., Woollings, T. and Caballero, R. (2014) Large-scale dynamics associated with clustering of extratropical cyclones affecting Western Europe. *Journal of Geophysical Research: Atmospheres*, 119, 704–713.

Ponce de León, S. and Bettencourt, J. (2021) Composite analysis of North Atlantic extra-tropical cyclone waves from satellite altimetry observations. *Advances in Space Research*, 68, 762–772.

Ponce de León, S. and Guedes Soares, C. (2014) Extreme wave parameters under North Atlantic extratropical cyclones. *Ocean Modelling*, 81, 78–88.

Rudeva, I. and Simmonds, I. (2015) Variability and trends of global atmospheric frontal activity and links with large-scale modes of variability. *Journal of Climate*, 28, 3311–3330.

Rulent, J., Calafat, F.M., Banks, C.J., Bricheno, L.M., Gommenginger, C., Green, J.A.M., Haigh, I.D., Lewis, H. and Martin, A.C.H. (2020) Comparing water level estimation in coastal and shelf seas from satellite altimetry and numerical models. *Frontiers in Marine Science*, 7, 1–14.

Sinclair, V., Belcher, S. and Gray, S. (2010) Synoptic controls on boundary-layer characteristics. *Boundary-Layer Meteorology*, 134, 387–409.

Smart, D.J. and Browning, K.A. (2014) Attribution of strong winds to a cold conveyor belt and sting jet. *Quarterly Journal of the Royal Meteorological Society*, 140, 595–610.

Sun, K., Li, L., Jagini, S. and Li, D. (2021) A satellite-data-driven framework to rapidly quantify air-basin-scale no_x emissions and its application to the po valley during the covid-19 pandemic. *Atmospheric Chemistry and Physics*, 21, 13311–13332.

Valiente, N.G., Saulter, A., Edwards, J.M., Lewis, H.W., Castillo Sanchez, J.M., Bruciaferri, D., Bunney, C. and Siddorn, J. (2021) The impact of wave model source terms and coupling strategies to rapidly developing waves across the north-west European shelf during extreme events. *Journal of Marine Science and Engineering*, 9, 403.

Vaughan, G., Methven, J., Anderson, D., Antonescu, B., Baker, L., Baker, T.P., Ballard, S.P., Bower, K.N., Brown, P.R.A., Chagnon, J., Choularton, T.W., Chylik, J., Connolly, P.J., Cook, P.A., Cotton, R.J., Crosier, J., Dearden, C., Dorsey, J.R., Frame, T.H.A., Gallagher, M.W., Goodliff, M., Gray, S.L., Harvey, B.J., Knippertz, P., Lean, H.W., Li, D., Lloyd, G., Martínez–Alvarado, O., Nicol, J., Norris, J., Öström, E., Owen, J., Parker, D.J., Plant, R.S., Renfrew, I.A., Roberts, N.M., Rosenberg, P., Rudd, A.C., Schultz, D.M., Taylor, J.P., Trzeciak, T., Tubbs, R., Vance, A.K., van Leeuwen, P.J., Wellpott, A. and Woolley, A. (2015) Cloud banding and winds in intense European cyclones: results from the DIAMET project. *Bulletin of the American Meteorological Society*, 96, 249–265.

Volonté, A., Turner, A.G., Schiemann, R., Vidale, P.L. and Klingaman, N.P. (2022) Characterising the interaction of tropical and extratropical air masses controlling East Asian summer monsoon progression using a novel frontal detection approach. *Weather and Climate Dynamics*, 3, 575–599.

WMO. (1970) *Commission for maritime meteorology. The Beaufort scale of wind force (technical and operational aspects).*

SUPPORTING INFORMATION

Additional supporting information can be found online in the Supporting Information section at the end of this article.

How to cite this article: Gentile, E. S., & Gray, S. L. (2023). Attribution of observed extreme marine wind speeds and associated hazards to midlatitude cyclone conveyor belt jets near the British Isles. *International Journal of Climatology*, 1–19. https://doi.org/10.1002/joc.7999